

Preparation of chains of magnetosomes, isolated from AMB-1 magnetotactic bacteria, yielding efficient treatment of tumors using magnetic hyperthermia

Edouard Alphandéry, François Guyot, Imène Chebbi

▶ **To cite this version:**

Edouard Alphandéry, François Guyot, Imène Chebbi. Preparation of chains of magnetosomes, isolated from AMB-1 magnetotactic bacteria, yielding efficient treatment of tumors using magnetic hyperthermia. International Journal of Pharmaceutics, 2012, 434 (1-2), pp.444 - 452. 10.1016/j.ijpharm.2012.06.015 . hal-01547081

HAL Id: hal-01547081

https://hal.sorbonne-universite.fr/hal-01547081

Submitted on 26 Jun 2017

HAL is a multi-disciplinary open access archive for the deposit and dissemination of scientific research documents, whether they are published or not. The documents may come from teaching and research institutions in France or abroad, or from public or private research centers.

L'archive ouverte pluridisciplinaire **HAL**, est destinée au dépôt et à la diffusion de documents scientifiques de niveau recherche, publiés ou non, émanant des établissements d'enseignement et de recherche français ou étrangers, des laboratoires publics ou privés.

Preparation of chains of magnetosomes, isolated from AMB-1 magnetotactic bacteria, yielding efficient treatment of tumors using magnetic hyperthermia

Edouard Alphandéry[+,⊥,*], *François Guyot*[+,x], *Imène Chebbi*[⊥],

[+]Institut de minéralogie et de physique des milieux condensés, Université Pierre et Marie Curie, UMR CNRS 7590, 4 Place Jussieu, 75005, Paris.

[⊥]Nanobacterie SARL, 36 boulevard Flandrin, 75016, Paris.

[x]Université Paris Diderot, Sorbonne Paris Cité, Institut de Physique du Globe de Paris, 1 Rue Jussieu, 75005, Paris

*CORRESPONDING AUTHOR CONTACT DETAILS:

E-MAIL edouardalphandery@hotmail.com

Phone: 33632697020.

Adresse: Nanobacterie, 36 boulevard Flandrin, 75016, Paris, France.

No fax.

ABSTRACT

Chains of magnetosomes isolated from AMB-1 magnetotactic bacteria by sonication at 30 W during 2 hours are tested for magnetic hyperthermia treatment of tumors. These chains are composed of magnetosomes, which are bound to each other by a filament made of proteins. When they are incubated in the presence of cancer cells and exposed to an alternating magnetic field of frequency 198 kHz and average magnetic field strength of 20 or 30 mT, they produce efficient inhibition of cancer cell proliferation. This behavior is explained by a high cellular internalization, a good stability in solution and a homogenous distribution of the magnetosome chains, which enables efficient heating. When the chains are heated during 5 hours at 90 °C in the presence of 1 % SDS, the filament binding the magnetosomes together is denatured and individual magnetosomes are obtained. By contrast to the chains of magnetosomes, the individual magnetosomes are prone to aggregation, are not stable in solution and do not produce efficient inhibition of cancer cell proliferation under application of an alternating magnetic field.

KEYWORDS

Magnetosomes, magnetotactic bacteria, cancer, tumor, chains of magnetosomes, individual magnetomes, alternating magnetic field, magnetic hyperthermia.

1. INTRODUCTION

Magnetic hyperthermia is a technique by which magnetic nanoparticles are either introduced or sent within tumors and heated under the application of an alternating magnetic field (AMF). The heat produced locally by the nanoparticles induces anti-tumoral activity. Magnetic hyperthermia has been used both on animal models and on humans to treat a series of different cancers, including breast cancer, [1, 2], prostate cancer, [3-6], glioblastoma, [7], and head and neck cancer, [8]. Until now, most of the iron oxide nanoparticles tested were chemically synthesized with either a superparamagnetic or a weakly ferrimagnetic behavior at physiological temperature, [9-12]. For an applied magnetic field of frequency and strength kept below a toxicity threshold of ~ 200 kHz and ~ 100 mT respectively, [13], the specific absorption rate (SAR) of the chemically synthesized nanoparticles is lower by a factor of 2 to 100 than that of the biologically synthesized nanoparticles, called magnetosomes, [9-11]. For this reason, there has been a surge of interest to carry out magnetic hyperthermia for cancer treatment using the magnetosomes, [14-18]. In fact, the magnetosomes are monodomain, well-crystallized nanoparticles surrounded by a lipidic membrane with the unique property of being usually arranged in chains. They are synthesized by a species of bacteria, called magnetotactic bacteria, which use them as a compass to navigate in the direction of the earth magnetic field in search for an optimum environment. In a previous study, [18], 1 mg of a suspension of chains of magnetosomes extracted from AMB-1 magnetotactic bacteria has been administered within breast tumors xeno-grafted under the skin of mice. After three applications of an alternating magnetic field during 20 minutes, tumors were totally eradicated in several mice. These results suggest that chains of magnetosomes extracted from AMB-1 magnetotactic bacteria are highly efficient for solid tumor treatment using magnetic hyperthermia, [18].

In this article, we examine if the efficiency of chains of magnetosomes extracted from AMB-1 magnetotactic bacteria, designated as CM, is solely due to the high SAR of the magnetosomes or if it also arises from other factors such as a homogenous distribution of the magnetosome chains within the tissue or a faculty of the magnetosome chains to internalize within the cancer cells. To know the

influence of the magnetosome chain arrangement on the efficiency of the therapy, we compare the properties of the chains of magnetosomes with those of individual magnetosomes, designated as IM, which are detached from the chains by heat and chemical treatments.

2. MATERIALS AND METHODS

2.1 Method used for the culture of the AMB-1 magnetotactic bacteria:

Magnetotactic bacteria belonging to the species *Magnetospirillum magneticum*, strain AMB-1, available at the ATCC under the reference 700264, were cultivated in a volume of 1 liter of bacterial growth medium. The cells were cultivated in micro-anaerobic conditions, *i. e.* in a culture medium that has not been degassed, but is closed and not in contact with oxygen. The culture of magnetotactic bacteria has been carried out in an incubator at 26 °C in a slightly modified MSGM liquid culture medium, whose composition is described below.

For a volume of 1 liter, the standard culture medium contains 0.68 g of monobasic potassium phosphate, 0.85 g of sodium succinate, 0.57 g of sodium tartrate, 0.083 g of sodium acetate, 225 µl of 0.2 % resazurine, 0.17 g of sodium nitrate, 0.04 g of L-ascorbic acid, 2 ml of a 10 mM solution of iron quinate, 10 mL of a solution of Woolf's vitamins and 5 mL of a solution of Woolf's minerals. The solution of iron quinate has been prepared by dissolving 0.19 g of quinic acid and 0.29 g of $FeCl_3$.6H2O in 100 ml of distilled water. The solution of Woolf's minerals contains in 1 liter of distilled water, 0.5 g of nitrilotriacetic acid (NTA, $C_6H_9O_6$), 1.5 g of magnesium sulfate heptahydrate ($MgSO_4.7H_2O$), 1 g of sodium chloride, 0.5 g of manganese sulfate monohydrate ($MnSO_4.H_2O$), 100 mg of iron sulfate heptahydrate ($FeSO_4.7H_2O$), 100 mg of cobalt nitrate heptahydrate ($Co(NO_3)_2.7H_2O$), 100 mg of calcium chloride ($CaCl_2$), 100 mg of zinc sulfate heptahydrate ($ZnSO_4.7H_2O$), 10 mg of copper sulfate pentahydrate ($CuSO_4.5H_2O$), 10 mg of aluminium potassium sulfate, 10 mg of potassium dodecahydrate ($AlK(SO_4).12H_2O$), 10 mg of boric acid (H_3BO_3), 10 mg of sodium molybdate dehydrate ($Na_2MoO_4.2H_2O$), 2 mg of sodium selenite (Na_2SeO_3), 10 mg of sodium tungstate dihydrate

88 ($Na_2WO_4.2H_2O$) and 20 mg of nickel chloride hexahydrate ($NiCl_2.6H_2O$). The solution of Woolf's
89 vitamins was prepared by dissolving in one liter of distilled water, 2.2 mg of folic acid (vitamin B9),
90 10.2 mg of pyridoxine (vitamin B6), 5.2 mg of riboflavin (vitamin B2), 5.2 mg of pantothenic acid
91 (vitamin B5), 0.4 mg of vitamin B12, 5.2 mg of amino-benzoic acid, 5.2 mg of thiotic acid and 900 mg
92 of potassium phosphate. The pH of the culture medium was adjusted to 6.85 by using a 1 M solution of
93 sodium hydroxide.

94 *2.2 Preparation of the different suspensions containing the extracted chains of magnetosomes and*
95 *individual magnetosomes:*

96 Two different types of magnetosomes have been isolated from AMB-1 magnetotactic bacteria, those
97 arranged in chains and those forming individual nanoparticles. To prepare them, the cells were first
98 harvested by centrifugation at 4 000 g during 20 minutes. The supernate was then removed and the cells
99 were re-suspended in deionized water. To extract the chains of magnetosomes, 1 ml of cell suspension
100 obtained as previously described was centrifugated again and re-suspended in a 10 ml tris-HCl buffer of
101 pH 7.4. The cellular suspension was then sonicated during 120 minutes at 30 W in order to lyse the cells
102 and collect the CM. After sonication, the suspension containing the CM was separated from the cellular
103 debris by positioning a strong neodynium magnet (0.1-1 T) next to the tube, and the magnetic material
104 was then harvested. The supernate containing the cellular debris and other organic molecules was
105 eliminated. CM were washed 10 to 20 times in deionized water at pH 7.4 and were then resuspended in
106 deionized water. To prepare the suspensions containing the IM, the suspension containing the CM was
107 heated during five hours at 90 °C in the presence of 1 % SDS. IM were separated from the biological
108 material remaining after the treatment by using a strong neodynium magnet (0.1-1T). The concentrations
109 in maghemite of the various suspensions containing CM and IM were measured by absorption at 480
110 nm, [18].

111 *2.3 Methods used for measuring the SAR and for heating the different suspensions of bacterial*
112 *magnetosomes:*

The SAR of suspensions of CM and IM were measured for bacterial magnetosomes, which were either able or unable to rotate under the application of an AMF, [16]. The amount of heat produced in the gel by the CM and IM was low under the application of an AMF of frequency 108 kHz and magnetic field strength kept below 36 mT, [16]. To enhance the magnetosome heating efficiency during the *in-vitro* and *in-vivo* heating experiments, the frequency of the AMF was therefore increased up to 198 kHz and the average magnetic field strength was kept below 30 mT to avoid the formation of eddy currents, which can induce toxicity. The average magnetic field strength was estimated from the variation with time of the magnetic field strength. It was measured using a 2D magnetic field probe designed by the company Fluxtrol. The value of the average magnetic field strength measured experimentally with this probe was 1.8 times lower than the theoretical value of the magnetic field, estimated using the relation $B = \mu_0 NI/L$, where $\mu_0 = 4\pi 10^{-7}$ is the vacuum permeability, N = 4 is the number of spires in the coil, I = 151, 300, 419 or 600 A is the amplitude of the alternating current flowing through the spires and L = 3.5 cm is the length of the coil (Suppl. table 1). The temperatures reached during the heating experiments were measured using a thermocouple microprobe (IT-18, Physitemp, Clifton, USA).

2.4 Percentage of inhibition and magnetization studies of HeLa and MDA-MB 231 cells incubated in the presence of the different suspensions of magnetosomes isolated from AMB-1 magnetotactic bacteria:

The HeLa and MDA-MB 231 cells were purchased from the ATCC. The cell lines were cultivated in Dulbecco's model modified Eagle's medium supplement, which contained 10% fetal calf serum, 2 mM L-glutamine, 1 mM sodium pyruvate, and 50 U/mL streptomycin (all purchased from Life Technologies Inc.). Cell viability was evaluated using the so-called MTT (microculture tetrazolium) assay, [19]. This technique measures the ability of mitochondrial enzyme to reduce 3-(4,5-dimethylthiazol-2-yl)-2,5-diphenyltetrazolium bromide (purchased from Sigma, St Louis, MO, USA) to purple formazan crystals. MDA-MB-231 and HeLa cells were seeded at a density of 2.10^4 cells per well in 96-well flat-bottom plates (Falcon, Strasbourg, France) and incubated in completed culture medium for 24 hours. Then, the culture medium was removed and replaced by 10 % FCS-medium containing CM or IM with different

concentrations in iron oxide (1 mg/mL, 500 µg/mL or 125 µg/mL). After 24 hours of incubation, the cells were exposed (or not) to an AMF of frequency 198 kHz and average magnetic field strength of ~ 20 mT or ~ 30 mT during 20 min. After having been exposed to the AMF, the cells were incubated at 37 °C in a 5 % CO_2 humidified atmosphere during 48 hours. Following the incubation, cells were washed with phosphate buffered saline solution (PBS, Life Technologies) and incubated with 100 µl of MTT (2 mg/ml, Sigma-Aldrich) for an additional 4 hours at 37 °C. The insoluble product was then dissolved by addition of 100 ml of DMSO (Sigma-Aldrich). The absorbance of the solubilized formazan pellet, which reflects the relative viable cell number, was measured at 540 nm using a Labsystems Multiskan MS microplate reader. The measurements were carried out on DMSO solubilized formazan pellets using cells washed with PBS as a control, [20]. The experiments were carried out in triplicates.

2.5 Internalization and magnetization studies of MDA-MB 231 cells incubated in the presence of various suspensions of magnetosomes:

5.10^5 MDA-MB-231 cells in suspension were mixed in 1 ml of a 10 % FCS-medium containing suspensions of CM or IM with a fixed concentration in iron oxide of 1 mg/ml. The cells were exposed (or not) to an AMF of frequency 198 kHz and average field strength of ~ 20 mT during 5, 10, 15 and 20 minutes. Following the application of the AMF, the MDA-MB-231 cells were collected with a strong neodynium magnet (0.1-1 T). For each sample, 10^4 cells were used to quantify the mass of iron oxide per cell. Solutions containing various concentrations of $FeCl_3$ mixed with potassium thiocyanate (2 M) were prepared for calibration. Solutions containing one volume of HCl (6 N) mixed with 20 volumes of H_2O_2 were added to the cells to dissolve the iron oxide into Fe^{3+} ions and to denature all biological material. The cells were further lysed by sonication during 30 minutes at 30 W (0 °C) and mixed with a solution of potassium thiocyanate (2 M), which induces the formation of a complex composed of Fe^{3+} and SCN^-. Quantification of iron oxide was estimated by absorption measurements at 480 nm (UVICON 923, Bio-Tek, Kontron Instrument, Italy). The untreated MDAMB-231 cells were used as reference. The experiments were carried out in triplicates.

2.6 In vitro Prussian blue assay:

MDA-MB-231 cells were seeded on Petri dishes (Ø 30 mm, density ~ 5. 10^5 cells per Petri dish), grown during 24 hours and incubated (or not) during 24 hours in the presence of suspensions of CM or IM at a concentration of 142 µg/mL. Cells were washed twice in PBS and fixed in 4 % paraformaldehyde (PFA) (Sigma) during 15 minutes at 4 °C. MDA-MB-231 cells were washed twice more time in PBS and were then stained with Perl's Prussian blue solution during 20 minutes at 37 °C in an atmosphere containing 5 % CO_2. Perl's Prussian blue solution was prepared by mixing two solutions of equal volumes containing 4 % potassium ferrocyanide and 4 % HCl. Staining (bright blue pigment: $Fe^{III}[Fe^{III}Fe^{II}(CN)_6]_3$) resulted from the reaction between Fe^{2+} or Fe^{3+} ions coming from the dissolved magnetosomes and the ferrocyanide ions. After having washed each Petri dish three times with PBS, Prussian blue staining was observed using an optical microscope. The experiments were carried out in triplicates.

2.7 Scanning electron microscopy, transmission electron microscopy and optical microscopy studies of MDA-MB 231 cells incubated in the presence of either chains of magnetosomes or individual magnetosomes:

Scanning electron microscopy (SEM) studies were carried out using a FEG-SEM ultra 55 from Zeiss equipped with an energy dispersive X-ray analysis system (EDX). The samples studied by SEM contained MDA-MB-231 cancer cells incubated during 24 hours in the presence of IM or CM. The cells were deposited on top of a carbon grid covered with a carbon film and fixed with NOVAprep, produced by Novacyt. Transmission electron microscopy (TEM) studies were also carried out using a JEOL 2100F-FEG operated at 200 kV. The samples studied by TEM contained 5 µl of suspensions of IM or CM deposited on top of a carbon grid. Optical microscopy was also used to visualize precipitated magnetosomes within MDA-MB 231 cells. For that, the cells were incubated in the presence (or not) of suspensions containing either CM or IM. The cells were stained with Prussian blue, which precipitates in the presence of iron, producing a blue color in the micrographs, which reveals the presence of iron.

3 RESULTS AND DISCUSSION

3.1 The different types of bacterial magnetosomes chosen for magnetic hyperthermia treatment of tumors:

In whole magnetotactic bacteria, the chains of magnetosomes only occupy a small portion of the total volume of a bacterium (~ 0.02 %). A TEM image of a typical AMB-1 magnetotactic bacterium is shown in Figure 1(a). Several chains of magnetosomes separated by more than ~ 100 nm are contained within this bacterium. Large regions of the bacterium are not occupied by chains of magnetosomes. Because of the low density of the chains of magnetosomes within whole magnetotactic bacteria, suspensions containing whole magnetotactic bacteria are expected to yield a low *in vivo* heating efficiency. In addition, the administration of whole inactive magnetotactic bacteria in humans is not recommended due to the presence of potentially toxic biologic materials such as bacterial DNA or endototoxins, [21]. For these two reasons, whole inactive magnetotactic bacteria were not tested in this study. In order to minimize the risks of toxicity and to enhance the heating efficiency, the bacterial magnetosomes were isolated from the bacteria.

The first type of bacterial magnetosomes tested for magnetic hyperthermia consisted of chains of magnetosomes extracted from AMB-1 magnetotactic bacteria, CM. Figure 1(b) shows a TEM image of a suspension of CM deposited on top of a carbon grid. The extraction of the chains of magnetosomes from the bacteria yields an increase in the concentration of the chains of magnetosomes (Figures 1(a) and 1(b)). The magnetosome chains also appear to be longer than in whole bacteria. When chains of magnetosomes are extracted from the magnetotactic bacteria, they interact with each other in such a way that they form longer chains. This type of interaction yields a homogeneous distribution of CM within the substrate (Figure 1(b)). To assess the stability of CM mixed in water, their zeta potential was measured as a function of pH by dynamic laser light scattering (DLS) on a Nano-ZS (Red Badge) ZEN 3600 device (Malvern Instruments, Malvern, UK). For a suspension of CM, which is homogenized by sonication, Figure 2(a) shows that the variations of the zeta potential as a function of pH is very similar

212 to that obtained for a non sonicated suspension of CM. This indicates the good stability of the
213 suspension of CM mixed in water. To examine if CM have kept the biological material surrounding
214 them after extraction, infra-red absorption measurements were carried out on CM. Figure 2(b) depicts
215 the infra-red absorption spectrum of a powder containing a lyophilized suspension of chains of
216 magnetosomes denatured and solubilized with KBr. It shows two absorption peaks at 1650 cm^{-1} (peak 1,
217 Figure 2(b)) and 1530 cm^{-1} (peak 2, Figure 2(b)), which arise from the Amide I and Amide II bands and
218 are due to the absorption of proteins, [21-23]. The peaks at 1250 cm^{-1} (peak 3, Figure 2(b)) and 1050
219 cm^{-1} (peak 4, Figure 2(b)) can either be attributed to the absorption of lipopolysaccharide (LPS) or
220 phospholipids [23,24], both located within the magnetosome membrane, [20]. The peak at 580 cm^{-1}
221 (peak 5, Figure 2(b)) is attributed to maghemite, [25]. These results suggest that both the filament
222 binding the magnetosomes together, which is made of proteins such as MamJ or Mam K, [26-28], and
223 the bilayer surrounding the individual magnetosomes, which is composed of LPS and phospholipids,
224 [29], are contained within CM. After extraction, the magnetosome chains have kept the lipid bi-layer
225 surrounding each magnetosome and the filament binding the magnetosomes together.

226 To obtain suspensions of magnetosomes, which are similar to the chemically synthesized iron oxide
227 nanoparticles, *i. e.* not arranged in chains, IM have been prepared by heating a suspension of CM at 90
228 °C during 5 hours in the presence of 1 % SDS. TEM images of a suspension of IM deposited on top of a
229 carbon grid are presented in Figures 1(c) and 1(d). It shows either assemblies of magnetosomes, which
230 are much more aggregated than the chains of magnetosomes (Figure 1(c)), or loops (Figure 1(d)). At pH
231 = 7, Figure 2(a) shows that suspensions of IM possess very different values of their zeta potential
232 depending on whether or not they are mixed homogeneously by sonication. When IM are mixed
233 homogenously in solution, they possess a negative zeta potential of ~ -35 mV at pH ~ 7, [30]. When
234 they are not sonicated, the IM zeta potential is 10 mV at pH ~ 7. The different values of the Zeta
235 potential suggest that IM easily form aggregates in solution and are therefore unstable in the absence of
236 sonication, [30]. The infra-red absorption spectrum of a powder containing a lyophilized suspension of

IM integrated in a KBr matrix is presented in Figure 2(b). It shows Amide I and Amide II peaks (peaks 1 and 2, Figure 2(b)), suggesting that most of the proteins contained in the filament binding the magnetosomes together have been removed. The relatively strong peaks at 1050 cm^{-1} and 1240 cm^{-1} suggest that the bi-layer surrounding each magnetosome has not been significantly removed during the heat treatment in the presence of a detergent.

3.2 SAR of the different suspensions of bacterial magnetosomes:

The SAR of suspensions containing IM and CM were measured in two situations in which the bacterial magnetosomes were either able or unable to rotate under the application of an AMF, [16]. For the bacterial magnetosomes mixed in water and able to rotate, Figures 3(a) and 3(b) show that the amount of heat produced by the CM is larger than that produced by the IM. This behavior could be explained by the fact that CM are less prone to aggregation and therefore rotate more easily than IM under the application of an AMF. This analysis is further supported by the TEM image presented in Figure 1(b), which clearly shows that CM do not aggregate by contrast to IM (Figure 1(c)). For the bacterial magnetosomes mixed in water, the higher value of the SAR obtained for CM compared with IM could therefore be explained by a contribution of the rotation to the heat production, which is more significant for CM than for IM. By contrast, when CM and IM are fixed (either in a gel or on a solid substrate, [16]), unable to rotate, mixed homogenously and exposed to the same AMF as above, IM produce a relatively similar amount of heat than CM (Figure 3), [16]. These results suggest that when the rotation of the magnetosomes is not taking part in the mechanism of heat production, which is most probably the case *in vivo*, the quantity of heat generated by CM or IM is not only due to the magnetosome SAR but also to the spatial distribution of the magnetosomes.

3.3 Percentage of inhibition of HeLa and MDA-MB-231 cells incubated in the presence of CM or IM:

To compare the anti-tumoral activity of CM with that of IM, CM and IM were incubated in the presence of HeLa and MDA-MB-231 cells. The percentage of inhibition of cellular proliferation was then

measured in the presence (or not) of an AMF. The results are presented for two suspensions of bacterial magnetosomes (CM or IM) with a concentration fixed at 0.125 mg/ml. In the absence of application of an AMF, the percentages of inhibition of MDA-MB-231 and HeLa cells incubated in the presence of CM or IM were as low as 2 % and 10 % (Figure 4(a)), respectively. When these cancer cells were incubated in the presence of the CM and exposed to an AMF of frequency 198 kHz and average magnetic field strength of 20 mT and 30 mT, the percentages of inhibition increased by factors of ~ 3 to ~ 5 for the HeLa cells and ~ 7 to ~ 16 for the MDA-MB-231 cells (Figure 4(a)). By contrast, when these cancer cells were incubated in the presence of IM and exposed to the same AMF as above, the percentage of inhibition of these cells remained almost identical (Figure 4(a)). A similar type of behavior was observed when MDA-MB6231 and HeLa cells were incubated in the presence of CM and IM at higher iron oxide concentrations of 1 mg/ml (Suppl. Fig. 1(a)) and 0.5 mg/ml (Suppl. Fig. 1(b)). These results indicate that under the application of an AMF, CM yield a higher percentage of cell inhibition than IM.

3.4 Penetration of the chains of magnetosomes within the cancer cells under the application (or not) of an alternating magnetic field:

We examine if the different efficiencies observed between CM and IM are due to a different faculty of penetration within the cancer cells of these two types of bacterial magnetosomes. We first study if the application of an AMF induces the internalization of CM or IM within the cancer cells. To be able to estimate the magnetization of MDA-MB-231 cells, the latter had to be kept free and not fixed. The cells were incubated in the presence of the CM and IM and exposed to the same AMF as above. The cancer cells were then washed with water to remove CM and IM located at their surface and the percentage of magnetic cells was then measured. Following application of an AMF of frequency 198 kHz during 5 to 20 minutes, Figure 4(b) shows that the mass of maghemite per magnetic cell is always much higher for the cells incubated in the presence of CM than for those incubated in the presence of IM. This result suggests that under the application of an AMF, CM penetrate much more within the cancer cells than

IM. Moreover, the high cellular magnetization, which can be reached in the presence of CM under the application of an AMF, could explain the high efficiency of CM for magnetic hyperthermia treatment of tumors.

We also study the internalization of CM and IM within the cancer cells as a function of the incubation time in the absence of an AMF. For that, the cells had to be fixed on top of a solid substrate. For a very short incubation time of less than 30 seconds, Figure 4(b) shows that neither CM nor IM penetrate within MDA-MB-231 cells. Suspensions containing CM and IM were then incubated in the presence of MDA-MB-231 cells for a longer incubation time of 24 hours. The cells were deposited on top of a carbon grid substrate and imaged under scanning electron microscopy. Figure 5(a) shows a portion of a typical MDA-MB-231 cell. Enlargements of two regions of the cell in which CM are observed are presented in Figures 5(b) and 5(c). Since CM are observed within intracellular vesicles, designated as V in Figure 5(b), which can be lysosomes or endosomes, CM are internalized within the cancer cell. The chain of magnetosome surrounded by a green box in Figures 5(c) and 5(d) contains two large magnetosomes at its end and several small magnetosomes at the middle. This type of magnetosome arrangement is clearly different from that observed for the magnetosome chains, which are not incubated in the presence of cancer cells (Figure 1(b)). It could be due to the degradation of the chains of magnetosomes by the cells following their internalization. Another reason why CM are internalized within the cells and not bound at the cell surface comes from the fact that the cells were washed prior to the observation by scanning electron microscopy. The presence of CM within the cells was further confirmed by EDX measurements, which revealed the presence of iron oxide in the region where CM were detected (Suppl. Fig. 3). By contrast to the behavior observed with CM, IM were not observed within the MDA-MB-231 cell (Suppl. Fig. 2). The EDX measurements confirmed this behavior (Suppl. Fig. 3). They showed that iron was not detected in the cellular regions with presumably no magnetosomes.

The internalization of CM within the cancer cells for a sufficiently long incubation time of 24 hours was further confirmed by optical microscopy. Figure 8 shows optical microscopy observations of MDA-MB-231 cells incubated in the absence of magnetosomes (Figure 8(a)), in the presence of CM during 24 hours (Figure 8(b)) or in the presence of IM during 24 hours (Figure 8(c)). For MDA-MB-231 cells incubated in the absence of magnetosomes or in the presence of IM, no Prussian blue coloration was observed within the cells. By contrast, for the MDA-MB-231 cells incubated in the presence of the CM, Prussian blue coloration was observed within the cells. These results agree with those presented above (Figures 5) and suggest that CM penetrate within the cells by contrast to IM, which remain located outside of the cells.

3.5 Explanation for the high efficiency of the chains of magnetosomes:

Altogether, these results indicate that CM penetrate more easily within the cancer cells than IM. While the internalization within the cancer cells did not occur with IM, it was observed for CM in two conditions, either when an AMF of 198 kHz and average field strength of 20 mT was applied during 5 to 20 minutes and/or when the cells were incubated with CM for a sufficiently long time of 24 hours. The internalization of CM within the cancer cells could occur by a mechanism of endocytosis or by effective diffusion through the cell membrane. The mechanism of effective diffusion through the cell membrane could be favored by a temperature increase taking place during the application of the AMF, which would make the cell membrane permeable. This result agrees with previous studies, which showed that negatively charged maghemite nanoparticles penetrate within cancer cells, [31]. Since intra-cellular heating presumably efficiently damages cellular components, it may be a more efficient mechanism of cell destruction than extra-cellular heating. The higher efficiency of CM compared with that of IM could therefore be explained by the fact that CM internalize within the cancer cells by contrast to IM, which mostly remain located outside of the cells. Poorly efficient internalization of IM may be related to the more aggregated state of IM compared with that of CM as was observed in two cases, *i. e.* when suspensions of CM and IM were deposited on top of a carbon grid (Figures 1(b) and 1(c)) and *in vivo*

when suspensions of CM and IM were administered within tumors xeno-grafted under the skin of mice and heated under the application of an AMF, [18]. A schematic summary showing the different distributions of CM and IM in the presence of cancer cells is proposed in Figures 9(a) and 9(b). The better internalization and more homogenous distribution of CM than IM could provide a reasonable explanation for the higher anti-tumoral efficiency observed for CM than for IM, [18].

4 Conclusion

In conclusion, we have studied two types of bacterial magnetosomes extracted from AMB-1 magnetotactic bacteria, the magnetosomes organized in chains and those forming individual magnetosomes detached from the chains by heat and chemical treatment. We have shown that chains of magnetosomes were more efficient than individual magnetosomes in inhibiting cancer cell proliferation under application of an alternating magnetic field. We have suggested that this increased efficiency was related to much less particle aggregation for the magnetosome chains than for the individual magnetosomes and as a consequence to a better faculty for the chains of magnetosomes than for the individual magnetosomes to internalize within the cancer cells. This paper clearly highlights the importance of nanoparticle distribution for efficient magnetic hyperthermia. It shows that the use of nanoparticles with high SAR is not sufficient to yield efficient magnetic hyperthermia.

ACKNOWLEDGMENTS

François Guyot does not claim any inventive contribution in this work. We thank the company NOVAcyt for giving us the NOVAprep product free of charge.

Figures:

Figure 1: (a) Transmission electron microscopy image of a typical whole inactive magnetotactic bacterium deposited on top of a carbon grid. The magnetosomes are designated by blue arrows. (b) Transmission electron microscopy image of suspensions of chains of magnetosomes, isolated from magnetotactic bacteria, and deposited on top of a carbon coated copper grid. (c) Transmission electron microscopy images of individual magnetosomes detached from the chains by heat and SDS treatment showing a typical aggregate. (d) Transmission electron microscopy images of individual magnetosomes detached from the chains by heat and SDS treatment showing a loop.

Figure 2: (a) Zeta potential of suspensions of chains of magnetosomes and individual magnetosomes as a function of pH. The measurements were carried out with suspensions containing bacterial magnetosomes either mixed homogenously by sonication or not mixed. (b) Infrared absorption spectra of powders containing lyophilized suspensions of CM or IM embedded within a KBr matrix.

Figure 3: (a) Specific absorption rate (SAR) of suspensions of chains of magnetosomes, which are able (or not if embedded in a gel or deposited on a solid substrate) to rotate under the application of an alternating magnetic field. (b) SAR of suspensions of individual magnetosomes, which are able (or not) to rotate under the application of an alternating magnetic field.

Figure 4: (a) Percentage of inhibition of HeLa and MDA-MB-231 cells incubated in the presence of CM and IM as a function of the magnetic field strength. (b) Mass of maghemite internalized within MDA-MB-231 cells incubated in the presence of IM and CM and exposed to an alternating magnetic field of frequency 198 kHz and average field strength of 20 mT during 5 to 20 minutes.

Figure 5: Scanning electron microscopy image of a MDA-MB-231 cell incubated in the presence of CM. V designates a vesicle.

Figure 6: Confocal optical microscopic images of cancer cells stained with Prussian blue and incubated in the absence of magnetosomes, (a), in the presence of CM, (b), and in the presence of IM, (c).

Figure 7: Conceptual summary describing the effect of aggregation on the penetration of magnetosomes within cancer cells. The magnetosomes are either CM, (a), or IM, (b).

401 **REFERENCES**

402 1. DeNardo, S.J., DeNardo, G.L., Natarajan, A., Miers, L.A., Foreman A.R., Gruettner C., Adamson
403 G.N., Ivkov R., 2007. Thermal Dosimetry Predictive of Efficacy of ^{111}In-ChL6 Nanoparticle AMF-
404 Induced Thermoablative Therapy for Human Breast Cancer in Mice. J. Nucl. Med. 48, 437-444.

405 2. Kikumori, T., Kobayashi, T., Sawaki, M., Imai, T., 2009. Anti-cancer effect of hyperthermia on
406 breast cancer by magnetite nanoparticle-loaded anti-HER2 immunoliposomes. Breast Cancer Res.
407 Treat. 113, 435-441.

408 3. Johannsen, M., Gnevekow, U., Eckelt, L., Feussner, A., Waldöfner, N., Scholz, R., Deger, S., Wust,
409 P., Loening, S.A., Jordan, A., 2005. Clinical hyperthermia od prostate cancer using magnetic
410 nanoparticles: Presentation of a new interstitial technique. Int. J. Hyperthermia 21, 637-647.

411 4. Johannsen, M., Gnevekow, U., Thiesen, B., Taymoorian, K., Cho, C.H., Waldöfner, N., Scholz, R.,
412 Jordan, A., Loening, S.A., Wust, P., 2007. Thermotherapy of Prostate Cancer Using Magnetic
413 Nanoparticles: Feasability, Imaging, and Three-Dimensional Temperature Distribution. European
414 Urology 52, 1653-1662.

415 5. Kawai, N., Ito, A., Nakahara, Y., Futakuchi, M., Shirai, T., Honda, H., Kobayasi, T., Kohri, K., 2005.
416 Anticancer Effect of Hyperthermia on Prostate Cancer Mediated by Mediated by Magnetite Cationic
417 Liposomes and Immune-Response Induction in Transplanted Syngeneic Rats. The Prostate. 64, 373-
418 381.

419 6. Kawai, N., Futakuchi, M., Yoshida, T., Ito, A., Sato, S., Naiki, T., Honda, H., Shirai, T., Kohri, K.,
420 2008. Effect of Heat Therapy Using Magnetic Nanoparticles Conjugated With Cationic Liposomes
421 on Prostate Tumor in Bone. The Prostate. 68, 784-792.

422 7. Maier-Hauff, K., Ulrich, F., Nestler, D., Niehoff, H., Wust, P., Thiesen, B., Orawa, H., Brudach, V.,
423 Jordan, A., 2011. Efficacy and safety of intratumoral thermotherapy using magnetic iron-oxide

nanoparticles combined with external beam radiotherapy on patients with recurrent glioblastoma multiforme. J. Neurooncol. 103, 317-324.

8. Zhao, Q., Wang, L., Cheng, R., Mao, L., Arnold, R.D., Howerth, E.W., Chen, Z.G., Platt, S., 2012. Magnetic Nanoparticle-Based Hyperthermia for Head and Neck Cancer in Mouse Models. Theranostics. 2, 113-121.

9. Hergt, R., Dutz. S., Müller, R., Zeisberger, M., 2006. Magnetic hyperthermia: nanoparticle magnetism and material development for cancer therapy. J. Phys.: Condens. Matter. S2919-S2934.

10. Hergt, R., Dutz, S., 2007. Magnetic particle hyperthermia-biophysical limitations of a visionary tumour therapy. J. Magn. Magn. Mat. 311, 187-192.

11. Hergt, R., Dutz, S., Röder, M., 2008. Effects of size distribution on hysteresis losses of magnetic nanoparticles for hyperthermia. J. Phys.: Condens. Matter. 385214.

12. Bordelan, D.E., Cornefo, C., Grüttner, C., Wesphal, F., Deweese, T.L., Ivkov, R., 2011. Magnetic nanoparticle heating efficiency reveals magneto-structural differences when characterized with wide ranging and high amplitude alternative magnetic fields. J. Appl. Phys. 109, 124904.

13. Ivkov, R., DeNardo, S.J., Daum, W., Foreman, A.R., Goldstein, R.C., Nemkov, V.S., DeNardo V., 2005. Application of High Amplitude Alternating Magnetic Fields for Heat Induction of Nanoparticles Localized in Cancer. Clin. Cancer Res. 11, 7093s-7103s.

14. Hergt, R., Hiergeist, R., Zeisberger, M., Schüler, D., Heyen, U., Hilger, I., Kaiser, W. A., 2005. Magnetic properties of bacterial magnetosomes as potential diagnostic and therapeutic tools. J. Magn. Magn. Matter. 293: 80-86.

15. Timko, M., Dzarova, A., Kovac, J., Skumiel, A., Józefcak, A., Hornowski, T., Gojżewski, H., Zavisova, V., Koneracka, M., Sprincova, A., Strbak, O., Kopcansky, P., 2009. Tomasovicova N, Magnetic properties and heating effect in bacterial magnetic nanoparticles. J. Magn. Magn. Matter. 321, 1521-1524.

16. Alphandéry, E., Faure, S., Chebbi, I., 2011. Treatment of cancer or tumor induced by the release of heat generated by various chains of magnetosomes extracted from magnetotactic bacteria and submitted to an alternative magnetic field. Int. Patent No. 061259.

17. Alphandéry, E., Carvallo, C., Menguy, N., Chebbi, I., 2011. Chains of Cobalt Doped Magnetosomes Extracted from AMB-1 Magnetotactic Bacteria for Application in Alternative Magnetic Field Cancer Therapy. J. Phys. Chem. C. 115, 11920-11924.

18. Alphandéry, E., Faure, S., Seksek, O., Guyot, F., Chebbi, I., 2011. Chains of Magnetosomes Extracted from AMB-1 Magnetotactic Bacteria for Application in Alternative Magnetic Field Cancer Therapy. ACSnano. 5, 6279-6296.

19. Mosmann, T., 1938. Rapid Colorimetric Assay for Cellular Growth and Survival: Application to Proliferation and Cytotoxicity Assays. J. Immunol. Methods. 65, 55-63.

20. Yoshino, T., Hirabe, H., Takahashi, M., Kuhara, M., Takeyama, H., Matsunaga, T., 2008. Magnetic Cell Separation Using Nano-Sized Bacterial Magnetic Particles With Reconstructed Magnetosome Membrane. Biotechnology and Bioengineering. 101, 470-477.

21. Diem, M., Bodydston-White, S., Chiriboga, L., 1999. Infrared Spectroscopy of Cells and Tissues: Shining Light onto a Novel Subject. Applied Spectroscopy. 53, 148A-161A.

22. Han, L., Li, S.Y., Yang, Y., Zhao, F.M., Huang, J., Chang, J., 2008. Research on the Structure and Performance of Bacterial Magnetic Nanoparticles. J. Biomat. Appl. 22, 433-448.

23. Song, H.P., Li, X.G., Sun, J.S., Xu, S.M., Han, X., 2008. Application of a magnetotactic bacterium, *Stenotrophomas* sp. to the removal of Au(III) from contaminated wastewater with a magnetic separator. Chemosphere. 72, 616-621.

24. Abramson, M.B., Norton, W.T., Katzman, R., 1965. Study of Ionic Structures in Phospholipids by Infrared Spectra. The Journal of Biological Chemistry. 240, 2389-2395.

25. Salazar, A., Morales, A., Marquez, M., 2011. Characterization of natural microcosms of estuarine magnetotactic bacteria. Dyna. 72-80.

26. Draper, O., Byrne, M.E., Li, Z., Keyhani, S., Barrozo, J.C., Jensen, G., Komeili, A., 2011. Mam K, A bacterial actin, forms dynamic filament in vivo that are regulated by the acidic proteins MamJ and Lim J. Mol. Microbiol. 82, 342-354.

27. Scheffel, A., Gruska, M., Faivre, D., Linaroudis, A., Plitzko, J., Schüler, D., 2006. An acidic protein aligns magnetosomes along a filamentous structure in magnetotactic bacteria. Nature. 440, 110-114.

28. Villanueva, A., Canete, M., Roca, A.G., Calero, M., Veintemillas-Verdaguer, S., Serna, C.J., Del Puerto Morales, M., Miranda, R., 2009. The influence of surface functionalization on the enhanced internalization of magnetic nanoparticles in cancer cells. Nanotechnology. 20, 115103.

29. Xie, J., Chen, K., Chen, X., 2009. Production, Modification and Bio-Applications of Magnetic Nanoparticles Gestates by Magnetotactic Bacteria. Nano. Res. 2, 261-278.

30. Sunderland, C.J., Steiert, M., Talmadge, J.E., Derfus, A.M., Barry, S.E., 2006. Targeted nanoparticles for detecting and treating cancer. Drug Dev. Res. 67, 70–93.

31. Wilhelm, C., Billotey, C., Roger, J., Pons, J.N., Bacri, J.C., Gazeau, F., 2003. Intracellular uptake of anionic superparamagnetic nanoparticles as a function of their surface coating. Biomaterials. 24, 1001-1011.

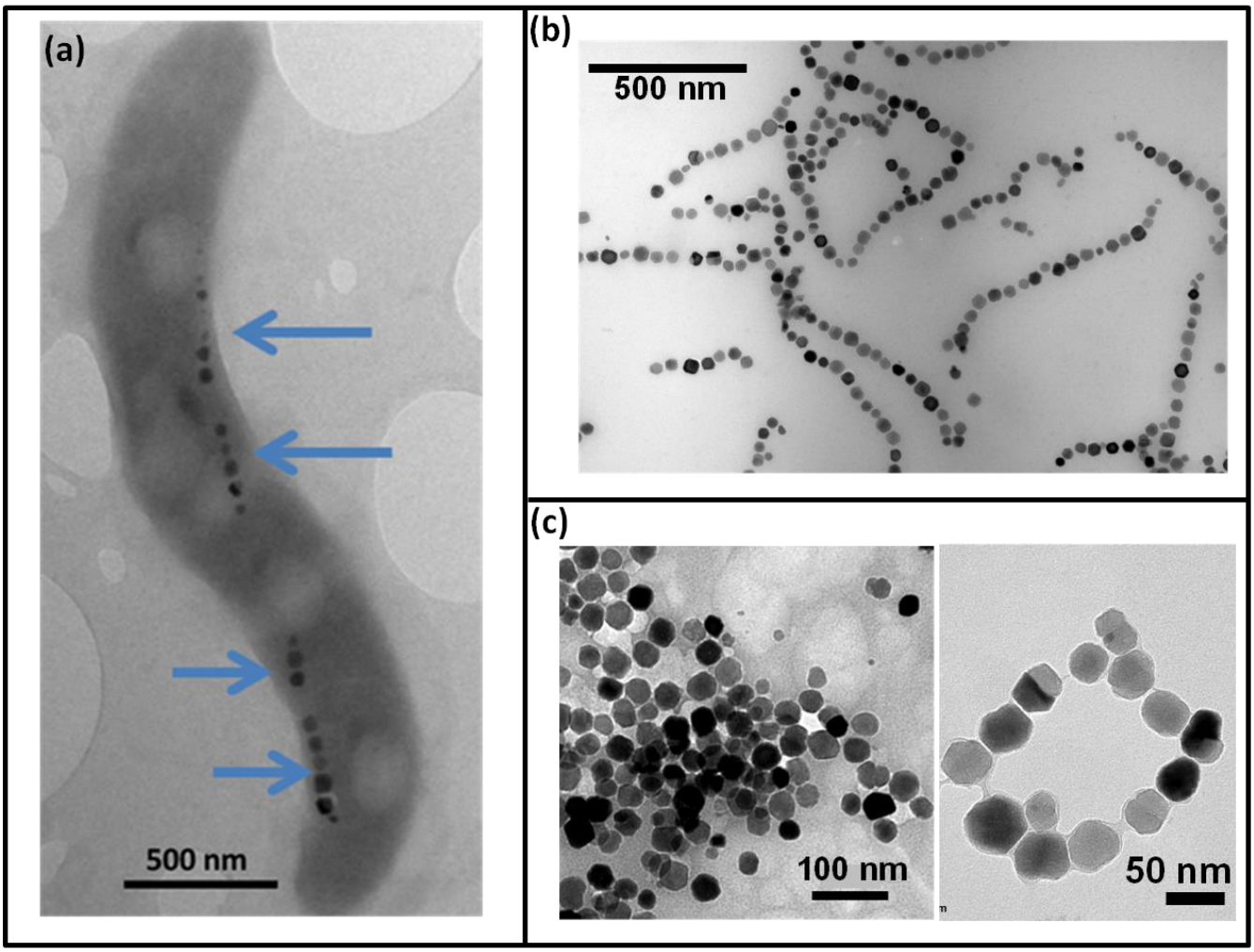


FIG. 1

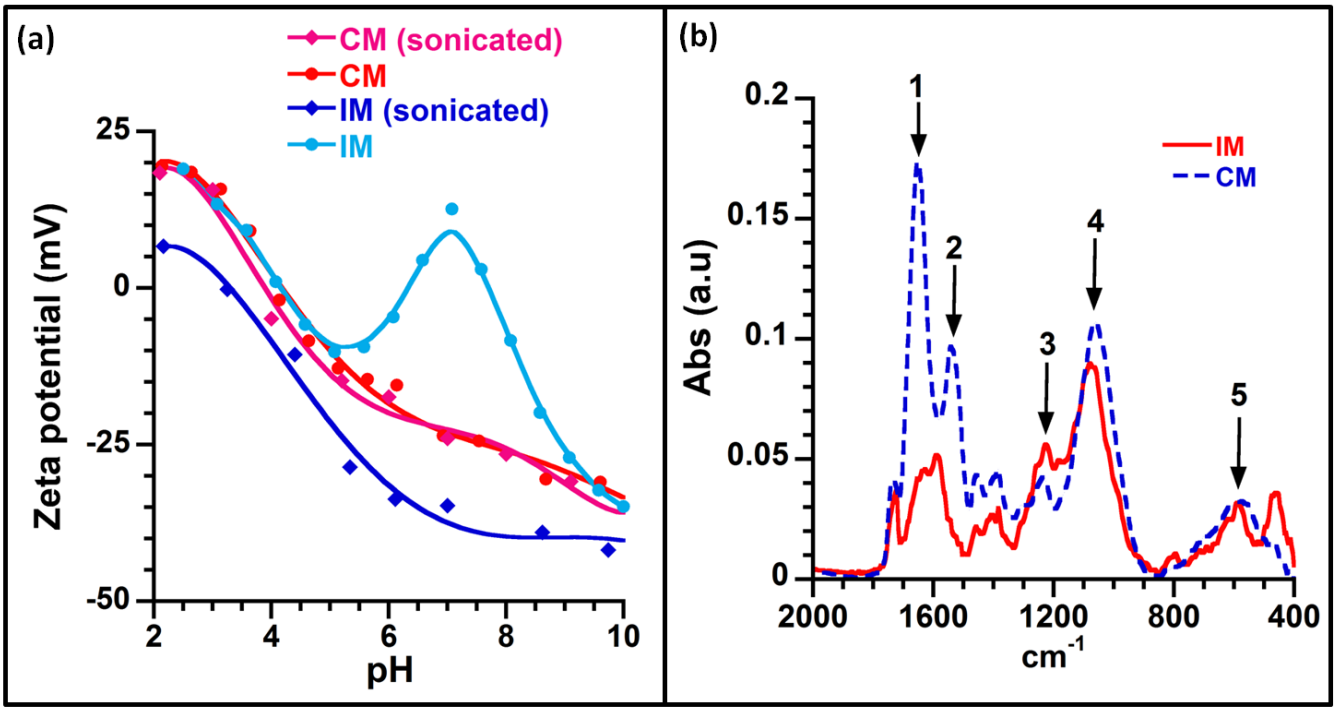

(a)
CM (sonicated)
CM
IM (sonicated)
IM
Zeta potential (mV)
25
0
-25
-50
2
4
6
8
10
pH
(b)
1
2
3
4
5
IM
CM
Abs (a.u)
0.2
0.15
0.1
0.05
0
2000
1600
1200
800
400
cm-1

FIG. 2

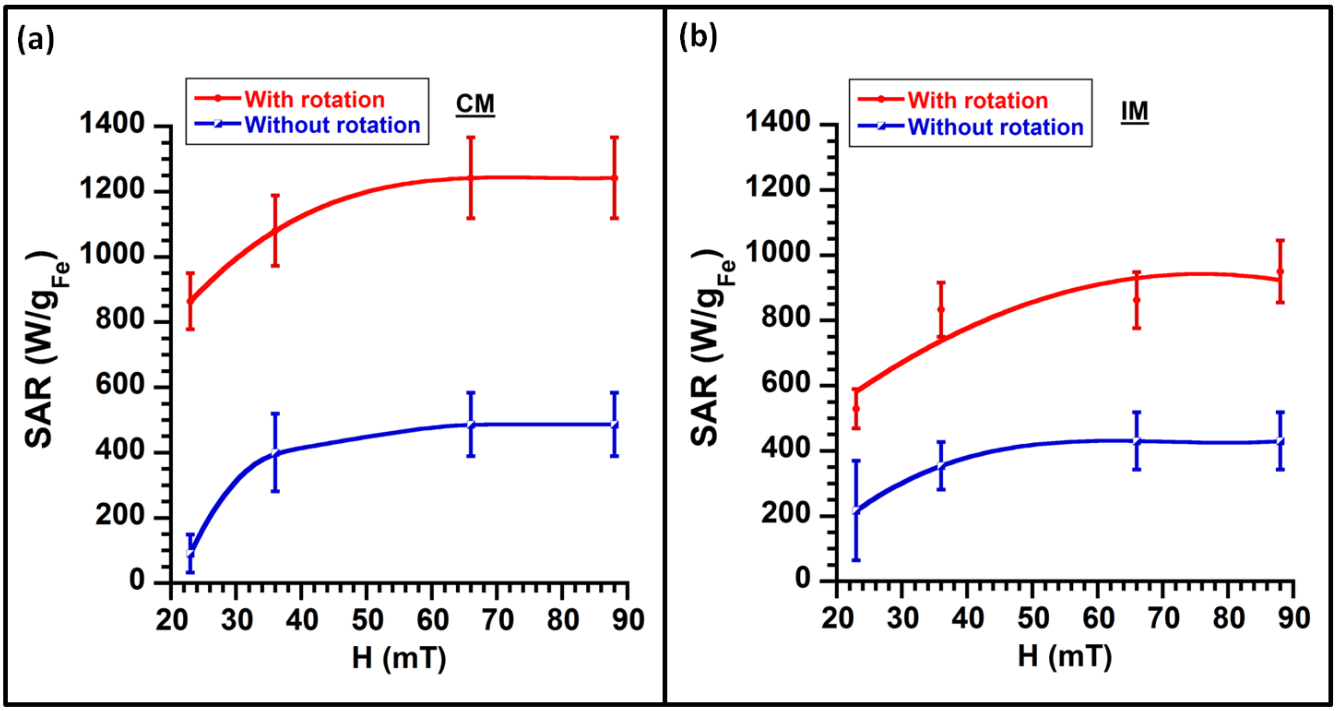

(a)
With rotation
Without rotation
CM
SAR (W/g$_{Fe}$)
H (mT)
(b)
With rotation
Without rotation
IM
SAR (W/g$_{Fe}$)
H (mT)

FIG. 3

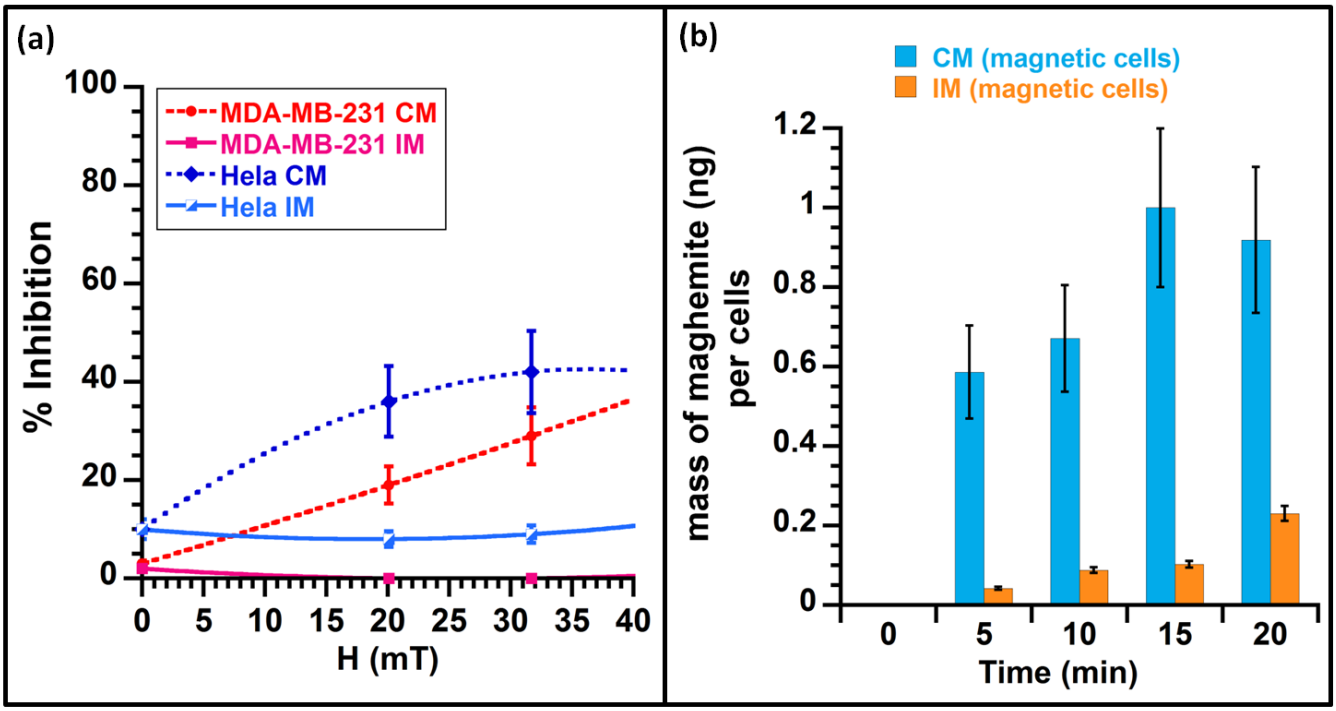

(a)
% Inhibition
H (mT)
MDA-MB-231 CM
MDA-MB-231 IM
Hela CM
Hela IM
(b)
mass of maghemite (ng) per cells
Time (min)
CM (magnetic cells)
IM (magnetic cells)

FIG. 4

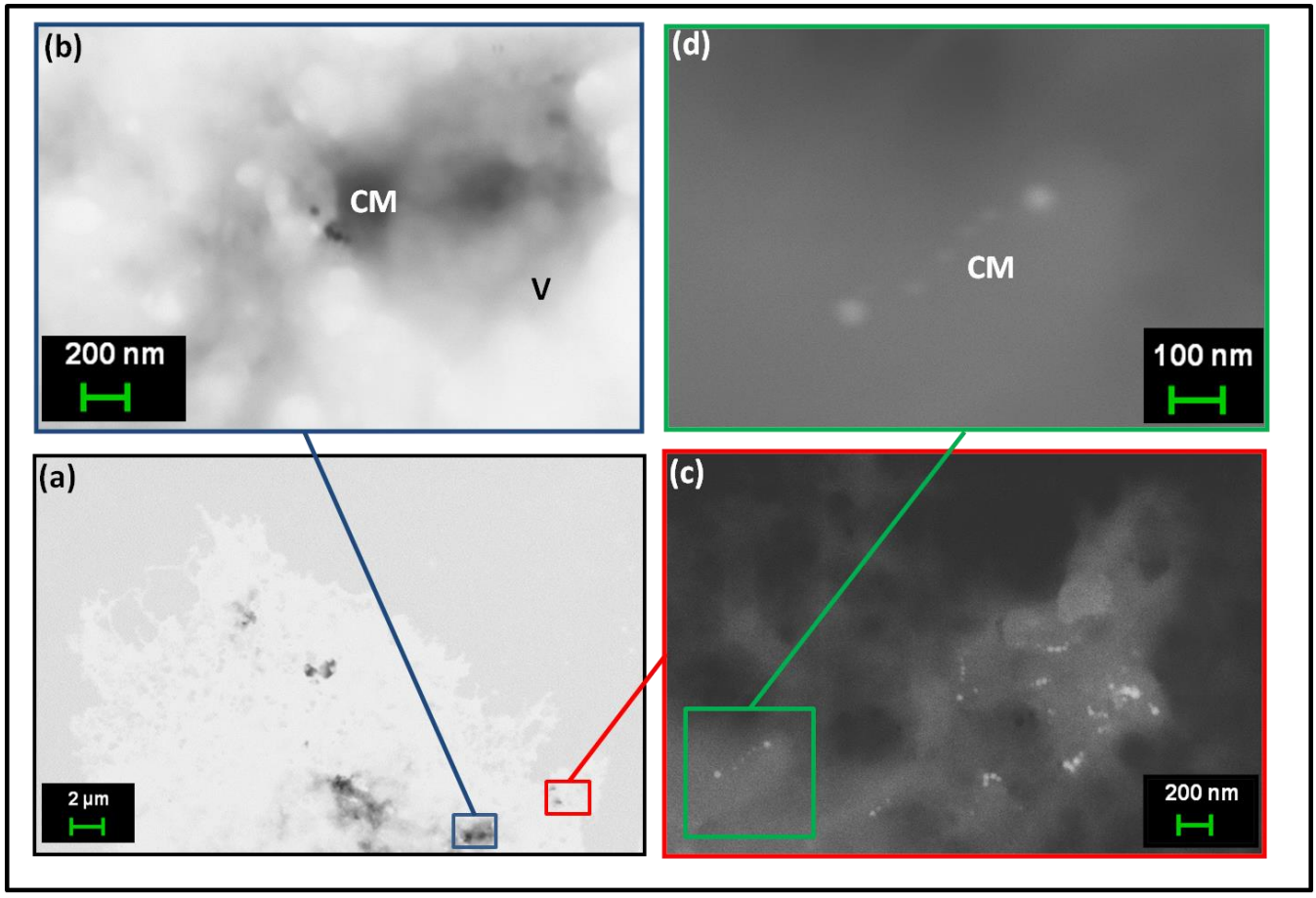


FIG. 5

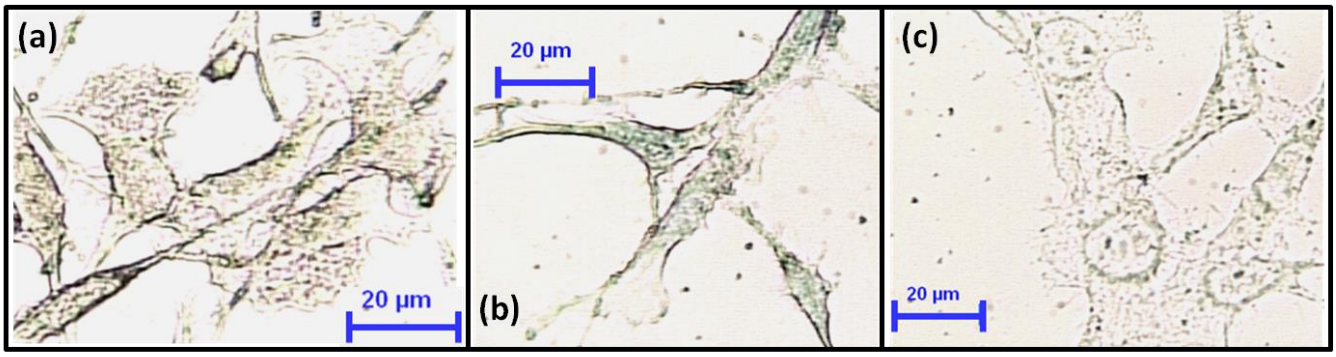


FIG. 6

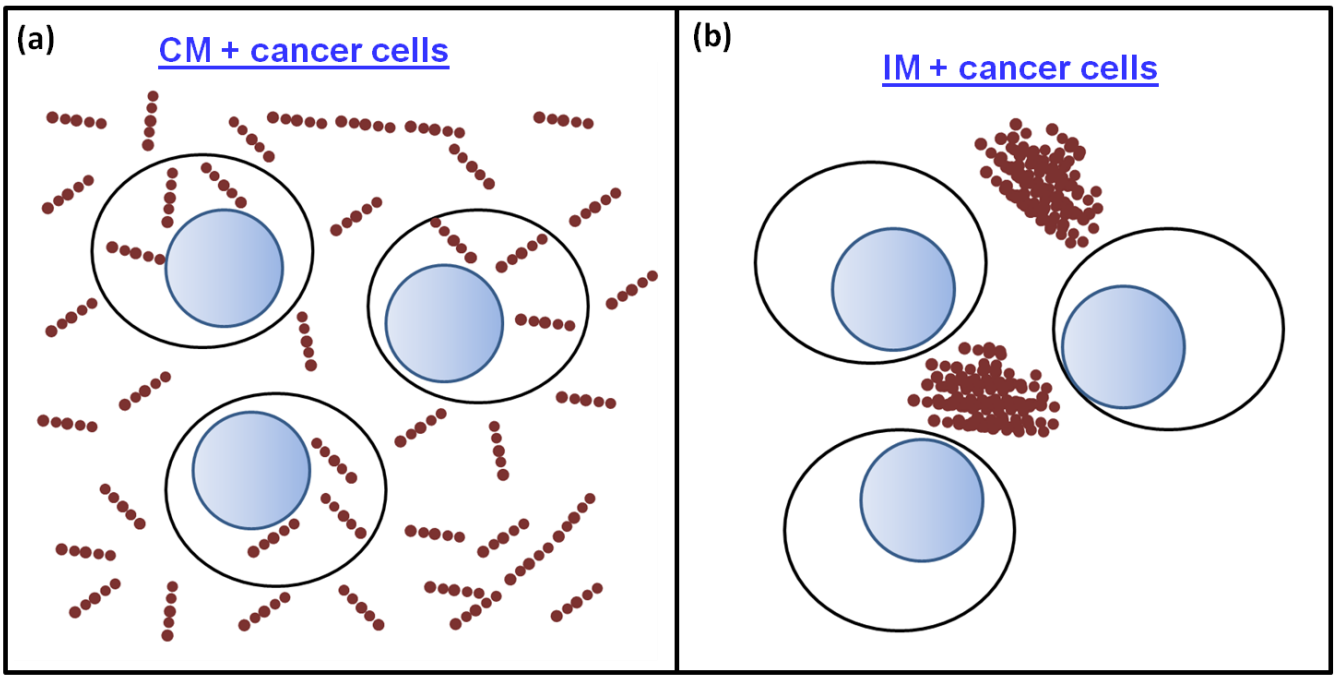


FIG. 7